Hindawi
Mathematical Problems in Engineering
Volume 2023, Article ID 5537632, 14 pages
https://doi.org/10.1155/2023/5537632

Research Article

Dynamics and Control of a Discrete Predator–Prey Model with Prey Refuge: Holling Type I Functional Response

Sarker Md. Sohel Rana and Md. Jasim Uddin

Department of Mathematics, University of Dhaka, Dhaka 1000, Bangladesh

Correspondence should be addressed to Md. Jasim Uddin; jasim.uddin@du.ac.bd

Received 14 August 2023; Revised 10 October 2023; Accepted 31 October 2023; Published 27 November 2023

Academic Editor: Sundarapandian Vaidyanathan

In this study, we examine the dynamics of a discrete-time predator–prey system with prey refuge. We discuss the stability prerequisite for effective fixed points. The existence criteria for period-doubling (PD) bifurcation and Neimark–Sacker (N–S) bifurcation are derived from the center manifold theorem and bifurcation theory. Examples of numerical simulations that demonstrate the validity of theoretical analysis, as well as complex dynamical behaviors and biological processes, include bifurcation diagrams, maximal Lyapunov exponents, fractal dimensions (FDs), and phase portraits, respectively. From a biological perspective, this suggests that the system can be stabilized into a locally stable coexistence by the tiny integral step size. However, the system might become unstable because of the large integral step size, resulting in richer and more complex dynamics. It has been discovered that the parameter values have a substantial impact on the dynamic behavior of the discrete prey–predator model. Finally, to control the chaotic trajectories that arise in the system, we employ a feedback control technique.

1. Introduction

The predator–prey model has both theoretical and real-world uses. A predator–prey model allows for the analysis of potential future events in a dynamic manner. There are several ways that interactions between various species can occur, including competition and predation. The predator–prey relationship is one of the most crucial relationships. Because of its well-known prevalence and significance, one of the key themes in mathematical ecology is the dynamic interaction of predator and prey. An important population dynamics model that looks at the dynamics of interacting groups [7] is the prey–predator paradigm. The Lotka–Volterra model [1, 2], has been employed by population dynamics to comprehend the interaction between ecological species [8–14]. Contrarily, discrete-time models have drawn great interest recently [15–17, 22, 23] because they are better suited to modeling populations with nonoverlapping generations and can produce complex dynamical behaviors than continuous part. The classic predator–prey relationship is given as follows:

$$\begin{aligned} \dot{x} &= x\widetilde{\Upsilon}\ (x,k) - y\widetilde{\Theta}(x), \\ \dot{y} &= y\left(-\delta + \widetilde{\Omega}(x)\right), \end{aligned} \tag{1}$$

with

$$x(0), y(0) > 0, \tag{2}$$

where the prey and predator population densities are represented by the time-dependent functions $x(t)$ and $y(t)$, respectively. All constant is assumed to be positive. The parameter k represents the carrying capacity. The constant δ represents the predator mortality rate. the functional response denoted by $\tilde{\Theta}(x)$, whereas $\tilde{\Omega}(x)$ represents the uptake functions.

Each population in an ecological system employs a unique strategy, such as refuging, clustering, etc., to locate food sources and defend itself. Numerous ecological features and elements are employed to build more accurate mathematical models. In population dynamics, the functional

response or the ratio of a predator's prey consumption to the density of prey per unit of time must be considered in every prey–predator contact [29, 30]. For the majority of arthropod predators, the functional response of the Holling type I, II [18], III, and IV is widely used. Later, the Lotka–Volterra model was investigated by Rosenzweig and MacArthur [24] using a logistic growth rate for the prey and a Holling type II functional response to account for the saturation of the predator. A limit cycle emerges when the stable fixed point experiences the Hopf bifurcation, which makes the Rosenzweig and MacArthur model one of the fundamental models since prey–predator cohabitation is not restricted to a stable fixed point. Rosenzweig and MacArthur model's discrete-time variant was examined by Hadeler and Gerstmann [25]. A straightforward discrete-time prey–predator model with Holling type I incidence was further examined by Danca et al. [10], who showed how chaotic processes may be seen in a straightforward discrete model. In their study of the Rosenzweig and MacArthur prey–predator model with Holling type I, Liu and Xiao [26] provided more evidence that the discrete system displays far richer dynamics than the continuous one. However, a prey refuge offers a more accurate prey–predator model because many prey populations have some sort of available refuge. Maynard [27] demonstrated that while a constant number of refugees of any size changed the neutrally stable behavior into a stable fixed point, the dynamics of the neutrally stable Lotka–Volterra model remained unchanged. In addition, Hassel [28] demonstrated that a big refuge in a model, which displays divergent oscillations in the absence of a refuge, substitutes a stable fixed for the oscillatory behavior. As a result, we note that numerous studies have demonstrated refugia's stabilizing influence on predator–prey relations. Prey refuge has been the subject of certain empirical and theoretical studies, and some of these studies have suggested that prey refuges have a stabilizing effect on predator–prey interactions and can effectively avoid the extinction of prey species [31–40, 47]. In a study by Seralan et al. [46], it was explored how the additive type Allee effect in the prey population affected the dynamic difficulties of the Ricker type predator–prey model. The analysis and exploration of the dynamics of a discrete Leslie–Gower predator–prey system with the Allee effect in the predator's population and with fear and Allee effect are observed in a study by Vinoth et al. [48, 49], respectively. A detailed exploration of discrete prey–predator model with multistability, torus doubling route to chaos is investigated in a study by Neverova et al. [50], Rajni and Ghosh [51], and Ghosh et al. [52].

According to Pusawidjayanti et al. [19], the following continuous predator–prey model's behavior has been examined as follows:

$$\begin{cases} \dot{x} = r_1 x - \dfrac{rx^2}{K} - \dfrac{(1-n)mxy}{1+x}, \\ \dot{y} = \dfrac{(1-n)cxy}{1+x} - r_2 y. \end{cases} \tag{3}$$

In a study by Khan [20], the author has considered the following discrete-time predator–prey model as follows:

$$\begin{cases} x_{t+1} = ax_t(1-x_t) - x_t y_t, \\ y_{t+1} = \dfrac{1}{\beta} x_t y_t, \end{cases} \tag{4}$$

where x_t and y_t, respectively, stand for the prey and predator populations. Parameters β and α are the predator and prey's natural growth rates. By introducing the Allee effect for the prey population in terms of dynamic behavior and Neimark–Sacker (N–S) bifurcation, Kangalgil [21] analyzed the discrete predator–prey model as follows:

$$\begin{cases} x_{t+1} = ax_t(1-x_t) - x_t y_t \left(\dfrac{x_t}{m + x_t} \right), \\ y_{t+1} = \dfrac{1}{\beta} x_t y_t. \end{cases} \tag{5}$$

Allee effect is referred to as $\frac{x}{m+x}$, where m is a positive constant. Utilizing discrete models is another approach to comprehend the challenging issue of prey and predator interaction. In the current work, modification of the model (5) is considered by introducing the prey refuge as follows:

$$\begin{aligned} x_{n+1} &= rx_n(1-x_n) - \alpha_a(1-m_a)x_n y_n, \\ y_{n+1} &= \beta_a(1-m_a)x_n y_n - \delta_a y_n. \end{aligned} \tag{6}$$

We focus on the dynamics of model (6) and few of the contributions made by this research include the followings:

(1) The suggested discrete-time prey–predator model displays complex dynamics than its continuous equivalent. We looked at the effect of prey refuge on the community of populations in the model.
(2) We look for potential fixed points in the stability of the system under study.
(3) The analytical result of period-doubling (PD) and N–S bifurcations has been proven.
(4) The N–S bifurcation has made the model chaotic, hence the state feedback control procedure has been applied to control it.
(5) Some numerical examples for our discrete-time predator–prey model with prey refuge have been supplied in order to confirm the validity of our theoretical results.

The remaining text is organized as follows: The fixed point, topological classes are discussed in Section 2. In Section 3, we analyze the likelihood that the model (6) will exhibit a PD or N–S bifurcation when a particular parametric condition is met. To support the conclusions of our analysis, in Section 4, we quantitatively demonstrate model dynamics

Table 1: Fixed point existence criteria of system (6).

Fixed points	Existence conditions
$\tilde{\zeta}_0$	Always
$\tilde{\zeta}_1$	$r>1$
$\tilde{\zeta}_2$	$r>1, m_a<\tilde{M}_0$

with bifurcation diagrams and phase portraits. In Section 5, we employ state feedback management strategies to control the chaotic model's disorder. In Section 6, a succinct discussion is offered.

2. Fixed Point Existence and Stability Analysis

2.1. Fixed Point Existence. The fixed points of system (6) are $\tilde{\zeta}_0=(0,0)$, $\tilde{\zeta}_1=(\frac{r-1}{r},0)$, and $\tilde{\zeta}_2=(x^*,y^*)$, where $x^*=\frac{-(1+\delta_a)}{\beta_a(-1+m_a)}$ and $y^*=\frac{r(1-x^*)-1}{\alpha_a(1-m_a)}$. Table 1 lists all of the fixed points' existence criteria.

where $\tilde{M}_0=\frac{\beta_a+r(1+\delta_a-\beta_a)}{\beta_a(1-r)}$

2.2. Analysis of Local Stability for Fixed Points. We evaluate the system's stability at the fixed points discovered in the system (6). It is important to note that, regardless of the magnitude of the predicted eigenvalues at the fixed point $\tilde{\zeta}(x,y)$, estimated eigenvalues have an effect on the fixed point's local stability.

The variational matrix of system (6) is shown as follows:

$$W_{\tilde{\zeta}}(x,y)=\begin{pmatrix}\widetilde{w_{11}} & \widetilde{w_{12}}\\ \widetilde{w_{21}} & \widetilde{w_{22}}\end{pmatrix}, \tag{7}$$

where

$$\begin{aligned}\widetilde{w_{11}} &= r(1-2x)-\alpha_a(1-m_a)y,\\ \widetilde{w_{12}} &= -\alpha_a(1-m_a)x,\\ \widetilde{w_{21}} &= \beta_a(1-m_a)y,\\ \widetilde{w_{22}} &= -\delta_a+\beta_a(1-m_a)x.\end{aligned} \tag{8}$$

The characteristic equation can be expressed as the following at $\tilde{\zeta}(x^*,y^*)$.

$$F_a(\lambda_a):=\lambda_a^2-\mathrm{Tr}\left(W_{\tilde{\zeta}}\right)\lambda_a+\mathrm{Det}\left(W_{\tilde{\zeta}}\right)=0, \tag{9}$$

where $\mathrm{Tr}(W_{\tilde{\zeta}})$ and $\mathrm{Det}(W_{\tilde{\zeta}})$ are given as follows:

$$\begin{aligned}\mathrm{Tr}\left(W_{\tilde{\zeta}}\right) &= \widetilde{w_{11}}+\widetilde{w_{22}},\\ \mathrm{Det}\left(W_{\tilde{\zeta}}\right) &= \widetilde{w_{11}}\widetilde{w_{22}}-\widetilde{w_{12}}\widetilde{w_{21}}.\end{aligned} \tag{10}$$

The eigenvalues of (9) can be derived as $\lambda_{a1,2}=\frac{\mathrm{Tr}(W_{\tilde{\zeta}})\pm\sqrt{\tilde{\Delta_{aa}}}}{2}$, where $\tilde{\Delta_{aa}}=\mathrm{Tr}(W_{\tilde{\zeta}})^2-4*\mathrm{Det}(W_{\tilde{\zeta}})$.

Let,

$$\begin{aligned}\widetilde{M_0} &= \frac{\beta_a+r(1+\delta_a-\beta_a)}{\beta_a(1-r)},\\ \widetilde{M_1} &= \frac{\beta_a+r(-1+\delta_a-\beta_a)}{\beta_a(1-r)},\\ \widetilde{M_2} &= \frac{2\beta_a+r(1+2\delta_a-3\beta_a)+r^2(-\delta_a+\beta_a)}{\beta_a(2-3r+r^2)},\\ \widetilde{M_3} &= \frac{3\beta_a-\beta_a\delta_a+r(-3-4\delta_a+\beta_a\delta_a+\beta_a)-\delta_a r^2}{\beta_a(3-\delta_a+\delta_1 r+r)},\\ \widetilde{M_4} &= \frac{r(2+\delta_a-\beta_a)+\beta_a}{\beta_a(1-r)}.\end{aligned} \tag{11}$$

One can get the stability requirement of fixed points $\tilde{\zeta}_0$, $\tilde{\zeta}_1$, and $\tilde{\zeta}_2$ easily from the Jury's criterion (see [45]) $F_a(-1)>0$, $F_a(0)-1<0$, $F_a(1)>0$ and proofs are omitted. Table 2 shows the stability conditions of fixed points, and Figures 1 and 2 show more information. The eigenvalues are real in the right part of the region in (m_a,r) space separated by the dashed line and on the opposite part, the eigenvalues are complex.

3. Bifurcation Analysis

3.1. Period-Doubling Bifurcation. We take the system (6) at the fixed point $\tilde{\zeta}_2(x^*,y^*)$ where the parameters $(r,a,\beta_a,\alpha_a,\delta_a)$ are chosen at random.

Let, $m_a=\tilde{M}_3=m_{aPD}$. Then, the eigenvalues of $W_{\tilde{\zeta}}$ are provided as follows:

$$\lambda_{a1}\left(\widetilde{M_3}\right)=-1, \text{and } \lambda_{a2}\left(\widetilde{M_3}\right)=-\frac{-6+\delta_a(-4+r)+r}{3+\delta_a}. \tag{12}$$

For $|\lambda_{a2}(\tilde{M}_3)\neq 1|$ to be implied as follows:

$$\frac{-\delta_a+\delta_a(-4+r)+r}{3+\delta_a}\neq\pm 1. \tag{13}$$

Next, we set $A(m_a)=W_{\tilde{\zeta}}$ and apply the transformations $\widehat{x}=x-x^*, \widehat{y}=y-y^*$. We relocate system (6)'s fixed point to the starting point. Consequently, the system (6) can be expressed as follows:

$$\begin{pmatrix}\widehat{x}\\ \widehat{y}\end{pmatrix}\to A(m_{aPD})\begin{pmatrix}\widehat{x}\\ \widehat{y}\end{pmatrix}+\begin{pmatrix}F_{x1}(\widehat{x},\widehat{y},m_{aPD})\\ F_{x2}(\widehat{x},\widehat{y},m_{aPD})\end{pmatrix}, \tag{14}$$

where $Y=(\widehat{x},\widehat{y})^T$ and

$$\begin{aligned}F_{x1}(\widehat{x},\widehat{y},m_{aPD}) &= \frac{1}{2}(-2r\widehat{x}^2-2\alpha_a(1-m_a)\widehat{x}\widehat{y}),\\ F_{x2}(\widehat{x},\widehat{y},m_{aPD}) &= \beta a(1-m_a)\widehat{x}\widehat{y}.\end{aligned} \tag{15}$$

Table 2: Analysis of system (6)'s local dynamics at fixed points $\tilde{\zeta}_i$ $(i=0,1,2)$.

Fixed points	The requisite condition(s) under which the mentioned fixed points exist	Behavior	Relative parametric requirements (regions in Figure 1)
$\tilde{\zeta}_0$	Always	Source	$r>1, \delta_a>1$
		Sink	$r<1, \delta_a<1$ (region 1)
		Saddle	$r<1, \delta_a>1$ or $r>1, \delta_a<1$ (regions 2–8)
		Nonhyperbolic	$r=1, \delta_a\neq 1$ (with fold bifurcation) $r\neq 1, \delta_a=1$ (with PD bifurcation)
$\tilde{\zeta}_1$	$r>1$	Source	$\max(\tilde{M}_0,\tilde{M}_2)<m_a<\tilde{M}_1, r>3$ (regions 5, 7)
		Sink	$\tilde{M}_0<m_a<\min(\tilde{M}_1,\tilde{M}_2), 1<r<3$ (region 2)
		Saddle	$m_a>\max(\tilde{M}_0,\tilde{M}_1), 1<r<3$ or $r>3, \tilde{M}_0<m_a<\tilde{M}_1$ (regions 6, 8)
		Nonhyperbolic	$r=3, \text{or} m_a=\tilde{M}_1$ (with PD bifurcation) $r=1, \text{or} m_a=\tilde{M}_0$ (with fold bifurcation)
$\tilde{\zeta}_2$	$r>1, m_a<\tilde{M}_0$	Sink	$\tilde{\Delta}_{aa}\geq 0, \tilde{M}_4<m_a<\tilde{M}_3,\ \tilde{\Delta}_{aa}<0, m_a>\tilde{M}_4$ (regions 5, 6)
		Source	$\tilde{\Delta}_{aa}\geq 0, m_a<\min(\tilde{M}_3,\tilde{M}_4)\ \tilde{\Delta}_{aa}<0, m_a<\tilde{M}_4$ (regions 7, 8)
		Saddle	$m_a>\tilde{M}_3$ (region 4)
		Nonhyperbolic	$\tilde{\Delta}_{aa}\geq 0, \mathrm{Tr}(W_{\tilde{\zeta}})\neq 0,2, m_a=\tilde{M}_3$ (with PD bifurcation), $\tilde{\Delta}_{aa}<0$, $m_a=\tilde{M}_4$ (with N–S bifurcation)

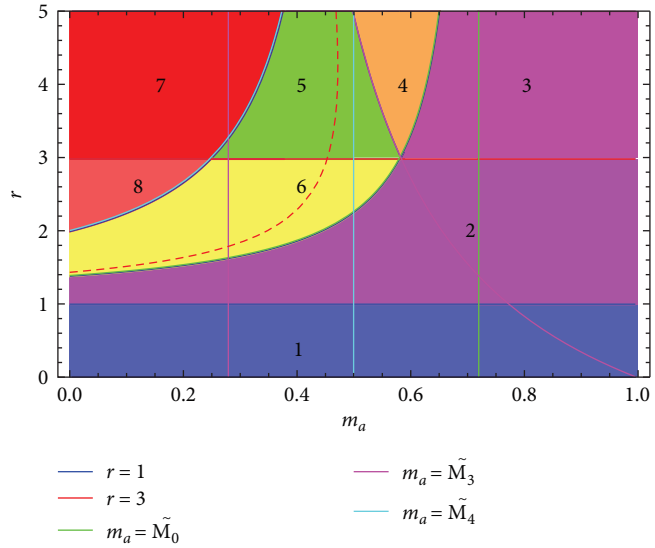

Figure 1: Stability regions of fixed points for model (6) with $\alpha_a=3.5, \beta_a=4.5, \delta_a=0.25$.

It is possible to express the system (6) as follows:

$$Y_{n+1}=AY_n+\frac{1}{2}B_e(Y_n,Y_n)+\frac{1}{6}C_e(Y_n,Y_n,Y_n)+O(\|Y_n\|^4). \tag{16}$$

As symmetric multilinear vector functions on $x,y,u\in\mathbb{R}^2$, $B_e(x,y)=\begin{pmatrix}B_{e1}(x,y)\\B_{e2}(x,y)\end{pmatrix}$, and $C_e(x,y,u)=\begin{pmatrix}C_{e1}(x,y,u)\\C_{e2}(x,y,u)\end{pmatrix}$ are defined as follows:

$$\begin{aligned}B_{e1}(x,y)&=\sum_{j,k=1}^{2}\frac{\delta^2F_{x1}(\xi,m_a)}{\delta\xi_j\delta\xi_k}\bigg|_{\xi=0}\quad x_jy_k=-2rx_1y_1-\alpha_a(1-m_a)(x_2y_1+x_1y_2),\\ B_{e2}(x,y)&=\sum_{j,k=1}^{2}\frac{\delta^2F_2(\xi,m_a)}{\delta\xi_j\delta\xi_k}\bigg|_{\xi=0}\quad x_jy_k=\beta_a(1-m_a)(x_2y_1+x_1y_2),\end{aligned} \tag{17}$$

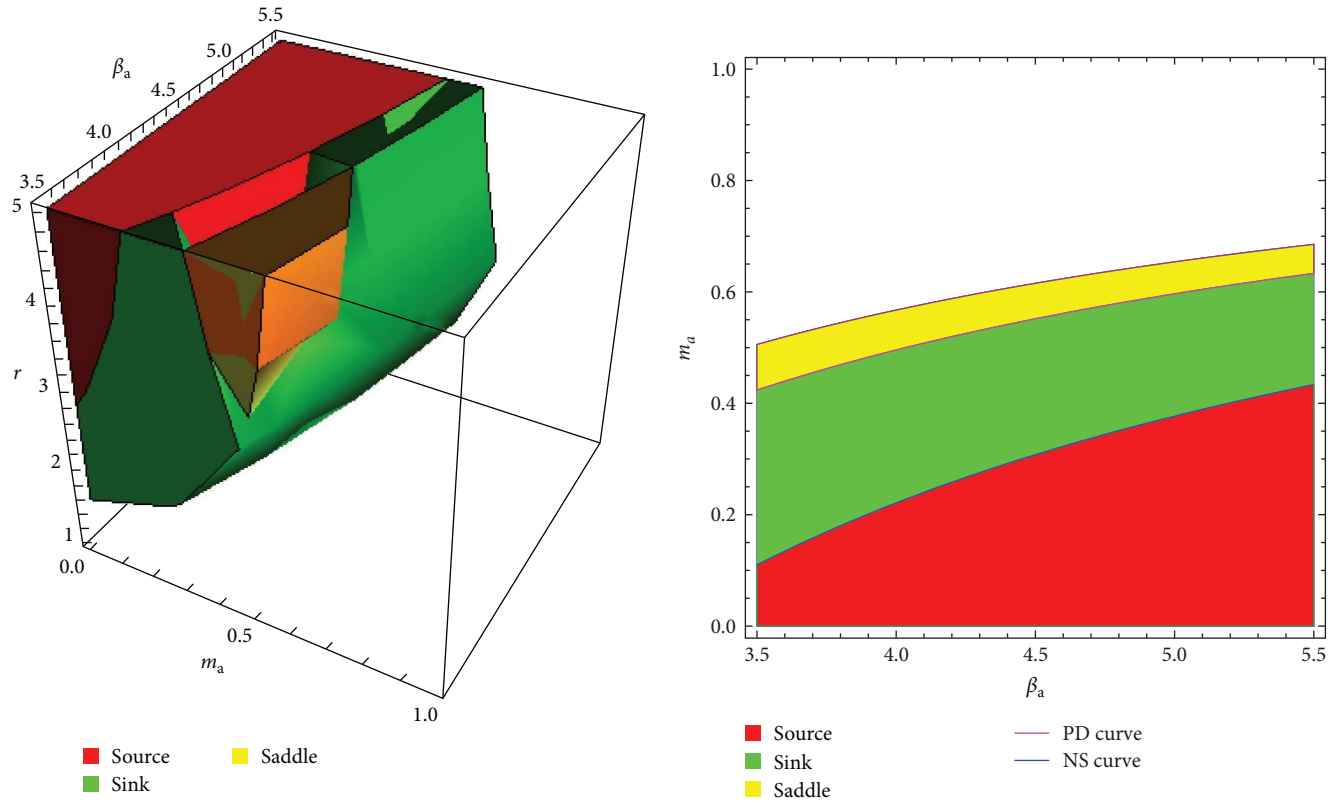

(a) (b)

FIGURE 2: Positive fixed point of the model (6) is categorized in (a) (m_a, r, β_a) space and (b) (β_a, m_a) space with $r = 3.60, \alpha_a = 3.5, \delta_a = 0.25$.

and

$$C_{e1}(x,y,u) = \sum_{j,k,l=1}^{2} \frac{\delta^2 F_{x1}(\xi, m_a)}{\delta\xi_j \delta\xi_k \delta\xi_l}\bigg|_{\xi=0} x_j y_k u_l = 0,$$
$$C_{e2}(x,y,u) = \sum_{j,k,l=1}^{2} \frac{\delta^2 F_{x1}(\xi, m_a)}{\delta\xi_j \delta\xi_k \delta\xi_l}\bigg|_{\xi=0} x_j y_k u_l = 0. \tag{18}$$

Let $\tilde{q}_1, \tilde{q}_2 \in \mathbb{R}^2$ the two eigenvectors of A and A^T should be represented by eigenvalue $\lambda_{a1}(m_{aPD}) = -1$ such that $A(m_{aPD})\tilde{q}_1 = -\tilde{q}_1$ and $A^T(m_{aPD})\tilde{q}_2 = -\tilde{q}_2$.

So, using straightforward calculation, we arrive at:

$$\widetilde{q_1} = \begin{pmatrix} 1 - \delta_a - \beta_a(-1 + m_a)x^* \\ \beta_a(-1 + m_a)y^* \end{pmatrix},$$
$$\widetilde{q_2} = \begin{pmatrix} 1 - \delta_a - \beta_a(-1 + m_a)x^* \\ -\alpha_a(-1 + m_a)x^* \end{pmatrix}. \tag{19}$$

For ensuring $\langle \tilde{q}_1, \tilde{q}_2 \rangle = 1$, where $\langle \tilde{q}_1, \tilde{q}_2 \rangle = \tilde{q_{11}}\tilde{q_{21}} + \tilde{q_{12}}\tilde{q_{22}}$, we have to utilize the normalized vector $\tilde{q}_2 = \gamma_{PD}\tilde{q}_2$, with $\gamma_{PD} = \frac{1}{(1-\delta_a-\beta_a(-1+m_a)x^*)^2 - \alpha_a\beta_a(-1+m_a)^2 x^* y^*}$.

We must examine the sign of $s_a(m_{aPD})$, the coefficient of the critical standard form [41], to establish the PD bifurcation's direction.

$$s_1(m_{aPD}) = \frac{1}{6}\langle \widetilde{q_2}, C_e(\widetilde{q_1}, \widetilde{q_1}, \widetilde{q_1}) \rangle - \frac{1}{2}\langle \widetilde{q_2}, B_e(\widetilde{q_2}, (A - I)^{-1} B_e(\widetilde{q_1}, \widetilde{q_1})) \rangle. \tag{20}$$

The direction and stability of PD bifurcation can be shown using the following theorem in light of the justification presented above.

Theorem 1. *For the fixed point $\tilde{\zeta}_2(x^*, y^*)$, assume that (13) is accurate. If $s_1(m_{aPD}) \neq 0$ and m_{aPD} fluctuate its value in a constrained vicinity to $\tilde{M}_3$, system (6) will experience a PD bifurcation at $\tilde{\zeta}_2(x^*, y^*)$. Additionally, if $s_1(m_{aPD})$ is positive or negative, period-2 orbits split apart from $\tilde{\zeta}_2(x^*, y^*)$ and become stable (or unstable).*

3.2. Neimark–Sacker Bifurcation. Next, we take the system (6) at the fixed point $\tilde{\zeta}_2(x^*, y^*)$ where the parameters $(r, a, \beta_a, \alpha_a, \delta_a)$ are chosen at random. Let $m_a = \tilde{M}_4 = m_{aNS} = \frac{-\beta_a - 2r + \beta_a r - \delta_a r}{\beta_a(-1+r)}$.

The system (6)'s eigenvalues are then complex, $\lambda_{1,2} \in \mathbb{C}$. Also,

$$\frac{d|\lambda_{ai}(m_a)|}{dm_a}\bigg|_{m_a = \widetilde{M_4}} = -\frac{-\beta_a(1+\delta_a)(-1+r)^2}{2(2+\delta_a)r} \neq 0,$$
$$-\left(trJ\left(\widetilde{M_4}\right)\right) \neq 0 \Rightarrow \frac{-5 + \delta_a(-3+r) + r}{2 + \delta_a} \neq 0, 1, \tag{21}$$

and

$$\lambda_a^k\left(\widetilde{M_4}\right) \neq 1; k = 1, 2, 3, 4. \tag{22}$$

Consider the case where $\tilde{q_1}, \tilde{q_2} \in \mathbb{R}^2$ be two eigenvectors of $A(m_{aNS})$ and $A^T(m_{aNS})$ for eigenvalue $\lambda_a(m_{aNS})$ and $\bar{\lambda_a}(m_{aNS})$ such that:

$$\begin{aligned} A(m_{aNS})\widetilde{q_1} &= \lambda_a(m_{aNS})\widetilde{q_1},\ A(m_{aNS})\bar{\tilde{q}_1} = \bar{\lambda_a}(m_{aNS})\bar{\tilde{q}_1} \\ A^T(m_{aNS})\widetilde{q_2} &= \bar{\lambda_a}(m_{aNS})\widetilde{q_2},\ A^T(m_{aNS})\bar{\tilde{q}_2} = \lambda_a(m_{aNS})\bar{\tilde{q}_2}. \end{aligned} \tag{23}$$

Therefore, by performing simple calculations, we find as follows:

$$\begin{aligned} \widetilde{q_1} &= \begin{pmatrix} -\delta_a - \lambda_a - \beta_a(-1+m_a)x^* \\ \beta_a(-1+m_a)y^* \end{pmatrix}, \\ \widetilde{q_2} &= \begin{pmatrix} -\delta_a - \bar{\lambda_a} - \beta_a(-1+m_a)x^* \\ -\alpha_a(-1+m_a)x^* \end{pmatrix}. \end{aligned} \tag{24}$$

To obtain $\langle \tilde{q_1}, \tilde{q_2} \rangle = 1$, where $\langle \tilde{q_1}, \tilde{q_2} \rangle = \tilde{q_{11}}\tilde{q_{21}} + \tilde{q_{12}}\tilde{q_{22}}$, we set the normalized vector $\tilde{q_2} = \gamma_{NS}\tilde{q_2}$, with $\gamma_{NS} = \frac{1}{(-\delta_a - \bar{\lambda} - \beta_a(-1+m_a)x^*)^2} - \alpha_a\beta_a(-1+m_a)^2x^*y^*$.

By taking into account how m_a can fluctuate close to m_{aNS} and for $z_a \in \mathbb{C}$, we can decompose $Y \in \mathbb{R}^2$ as $Y = z_a q_1 + \bar{z_a}\bar{q_1}$. $z_a = \langle q_2, Y \rangle$ is the exact formulation of z_a. Thus, for $|m_a|$ close to m_{aNS}, the system (6) switched to the following system as follows:

$$z_a \longmapsto \mu(m_a)z_a + \widehat{h}(z_a, \bar{z_a}, m_a), \tag{25}$$

where $\lambda(m_a) = (1 + \widehat{\varphi_a}(m_a))e^{i\theta(m_a)}$ with $\widehat{\varphi_a}(m_{aNS}) = 0$ and $\widehat{h}(z_a, \bar{z_a}, m_a)$ is an easily computed complex-valued function. When Taylor expansion is used on the function $\widehat{h}$, we get:

$\widehat{h}(z_a, \bar{z_a}, m_a) = \sum_{k+l\geq 2} \frac{1}{k!l!}\widehat{h}_{kl}(m_a)z_a^{k-l}$ with $\widehat{h}_{kl} \in \mathbb{C}, k, l = 0, 1, \ldots$.

Symmetric multilinear vector functions can be used to define the Taylor coefficients.

$$\begin{aligned} \widehat{h}_{20}(m_{aNS}) &= \langle q_2, B_e(q_1, q_1)\rangle, \\ \widehat{h}_{11}(m_{aNS}) &= \langle q_2, B_e(q_1, \bar{q_1})\rangle, \\ \widehat{h}_{02}(m_{aNS}) &= \langle q_2, B_e(\bar{q_1}, \bar{q_1})\rangle, \\ \widehat{h}_{21}(m_{aNS}) &= \langle q_2, C_e(q_1, q_1, \bar{q_1})\rangle. \end{aligned} \tag{26}$$

The first Lyapunov coefficient $s_2(m_{aNS})$ sign determines the N–S bifurcation's direction, which is given by the expression as follows:

$$\begin{aligned} s_2(m_{aNS}) = &\ \mathrm{Re}\left(\frac{\lambda_{a2}\widehat{h}_{21}}{2}\right) - \mathrm{Re}\left(\frac{(1-2\lambda_{a1})\lambda_{a2}{}^2}{2(1-\lambda_{a1})}\widehat{h}_{20}\widehat{h}_{11}\right) \\ &- \frac{1}{2}\left|\widehat{h}_{11}\right|^2 - \frac{1}{4}\left|\widehat{h}_{02}\right|^2 \end{aligned} \tag{27}$$

In light of the preceding explanation, the following theorem can be utilized to show the direction and stability of N–S bifurcation.

Theorem 2. *Assume that (21) is true and that $s_2(m_{aNS}) \neq 0$ is true. If the value of m_a fluctuates in a specific area around $\tilde{M}_4$, system (6) experiences a N–S bifurcation at $\tilde{\zeta_2}(x^*, y^*)$. Additionally, if $s_2(m_{aNS})$ is negative (resp. positive) and the N–S bifurcation is supercritical (resp. subcritical), a unique invariant closed curve that is attracting (resp. repelling) bifurcates from $\tilde{\zeta_2}(x^*, y^*)$ as well.*

4. Quantitative Study

In order to support our theoretical findings and demonstrate some novel, intriguing complex dynamical behaviors present in system (6), numerical simulation work has been done to exhibit bifurcation diagrams, phase portraits, Lyapunov exponents, and fractal dimension (FD) of system (6). Before presenting all the scenarios, we discuss the FD first.

4.1. Fractal Dimension. The idea of FD is frequently used in the context of dynamical systems to describe the complexity and self-similarity of the structures inside the system. FD gives an indication of how a set fills space, capturing complex patterns and imperfections that may not be well captured by traditional Euclidean geometry. The FDs measurement, which is defined by Cartwright [42], is used to determine a model's chaotic attractors.

$$\widehat{H}_{fd} = k + \frac{\sum_{j=1}^{k} \mathrm{ttt}_j}{|\mathrm{ttt}_{k+1}|}, \tag{28}$$

where k is the largest integer number such that $\sum_{j=1}^{k} \mathrm{ttt}_j \geq 0$ and $\sum_{j=1}^{k+1} \mathrm{ttt}_j < 0$ and tt_j's are Lyapunov exponents. Now, the model (6)'s fractal dimensions structure is given as follows:

$$\widehat{H}_{fd} = 2 + \frac{\mathrm{ttt}_1}{|\mathrm{ttt}_2|}. \tag{29}$$

Given that the chaotic dynamics of the model (6) (Figure 3) are quantified with the sign of FD (Figure 4(d)), it is inevitable that the dynamics of the model stabilize as the parameter m_a increases.

In the following situations, we take into account the bifurcation parameters:

Scenario (i) ranging m_a between the ranges of 0 and 1 and fixing other parameters as $r = 3.55, \alpha_a = 3.5, \beta_a = 4.5, \delta_a = 0.25$.

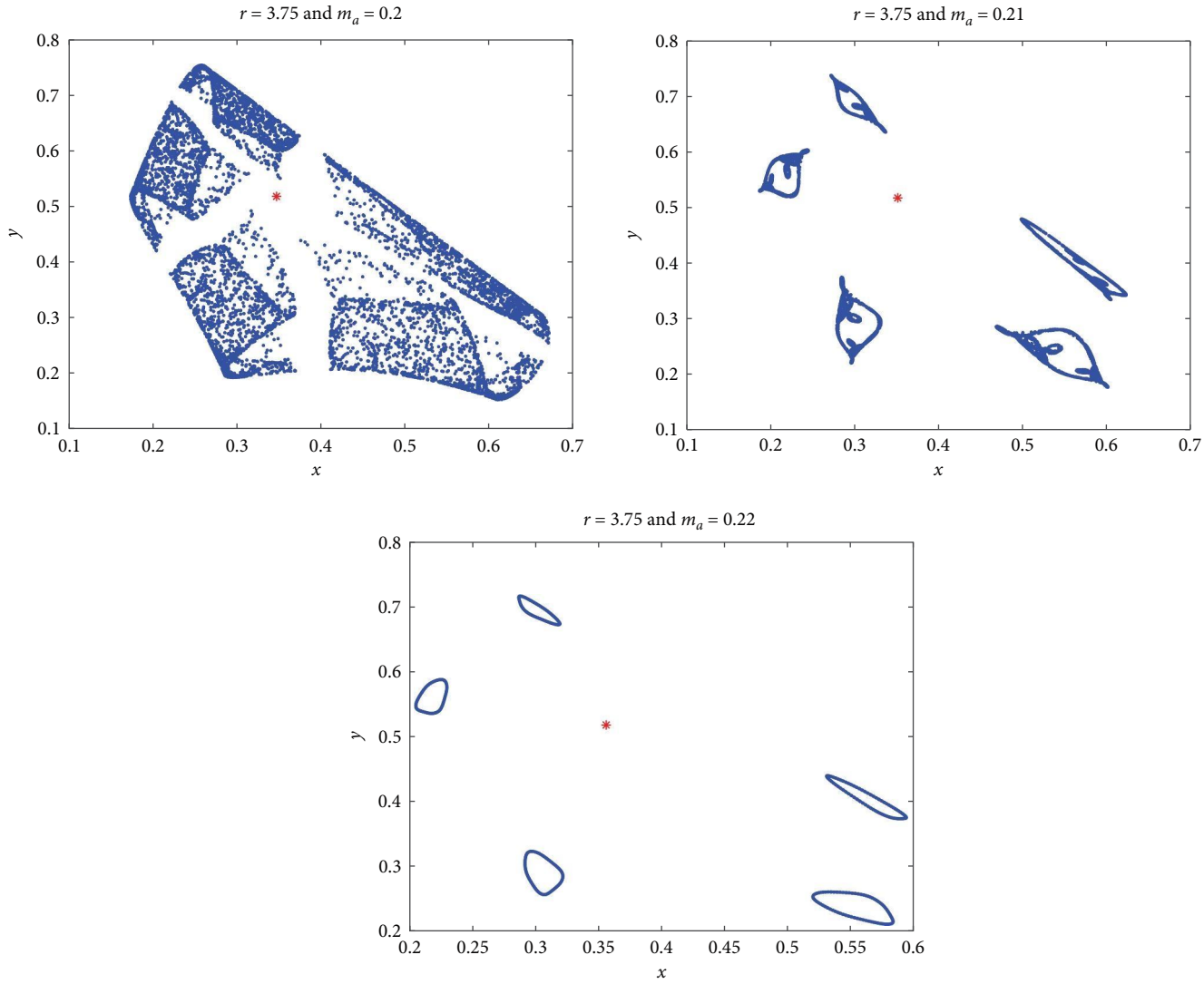

FIGURE 3: The phase diagram for altering the input of m_a.

Scenario (ii) ranging m_a between the ranges of 0 and 1 and fixing other parameters as $r = 3.75, \alpha_a = 3.5, \beta_a = 4.5, \delta_a = 0.25$.

Scenario (iii) ranging β_a between the ranges of 3.5 and 3.75 and fixing other parameters as $r = 3.75, \alpha_a = 3.5, m_a = 0.125, \delta_a = 0.25$.

For scenario (i), Figures 5(a) and 5(b) show the bifurcation diagrams of system (6) in the $(m_a - x)$ and $(m_a - y)$ planes. We notice that an N–S bifurcation emerges at $m_a = m_{aNS} = 0.303922$ around the fixed point $(0.399061, 0.465191)$ of system (6). At $m_a = m_{aNS}$, we get eigenvalues $\lambda_{a1,a2} = 0.291667 \pm 0.95652i$ and

$$\begin{aligned} &\frac{d|\lambda_{ai}(m_a)|}{dm_a}\Big|_{m_a = m_{aNS}} = -2.28961 \neq 0, \\ &-\left(tr\left(J_{\widetilde{M_4}}\right)\right)\Big|_{m_a = m_{aNS}} \neq 0 \Rightarrow = -0.58333 \neq 0, 1. \end{aligned} \tag{30}$$

The Taylor coefficients are given by $\widehat{h}_{20} = -1.47917 - 0.476808i$, $\widehat{h}_{11} = 2.21875 - 4.27194i$, $\widehat{h}_{02} = 5.91667 + 5.51551i$, $\widehat{h}_{21} = 0$ and $s_2(m_{aNS}) = -32.9831$. The N–S bifurcation is supercritical as a result, which confirms Theorem 2.

The calculated maximum Lyapunov exponent corresponding to Figures 5(a) and 5(b) is shown in Figure 5(c). The chaotic zone has stable fixed points or stable periodic windows as a result of certain Lyapunov exponents being positive and some being negative, as shown in Figure 5(c). The diagrams, as shown in Figures 5(a) and 5(b), demonstrate that the fixed point $\tilde{\zeta}_2$ of system (6) is unstable up to a scale factor of $m_a = 0.303922$ but becomes stable as the scale factor increases. Figure 6 is arranged with the phase portraits related to Figures 5(a) and 5(b) for different values of m_a; it unmistakably illustrates the procedure by which a smooth invariant circle deviates from the steady fixed point.

For scenario (ii), Figures 4(a) and 4(b) show the bifurcation diagrams of system (6) in the $(m_a - x)$ and $(m_a - y)$ planes. We observe that an N–S bifurcation emerges at $m_a = m_{aNS} = 0.318182$ near the fixed point $(0.407407, 0.512169)$ of system (6). At $m_a = m_{aNS}$, we find $\lambda_{a1,a2} =$

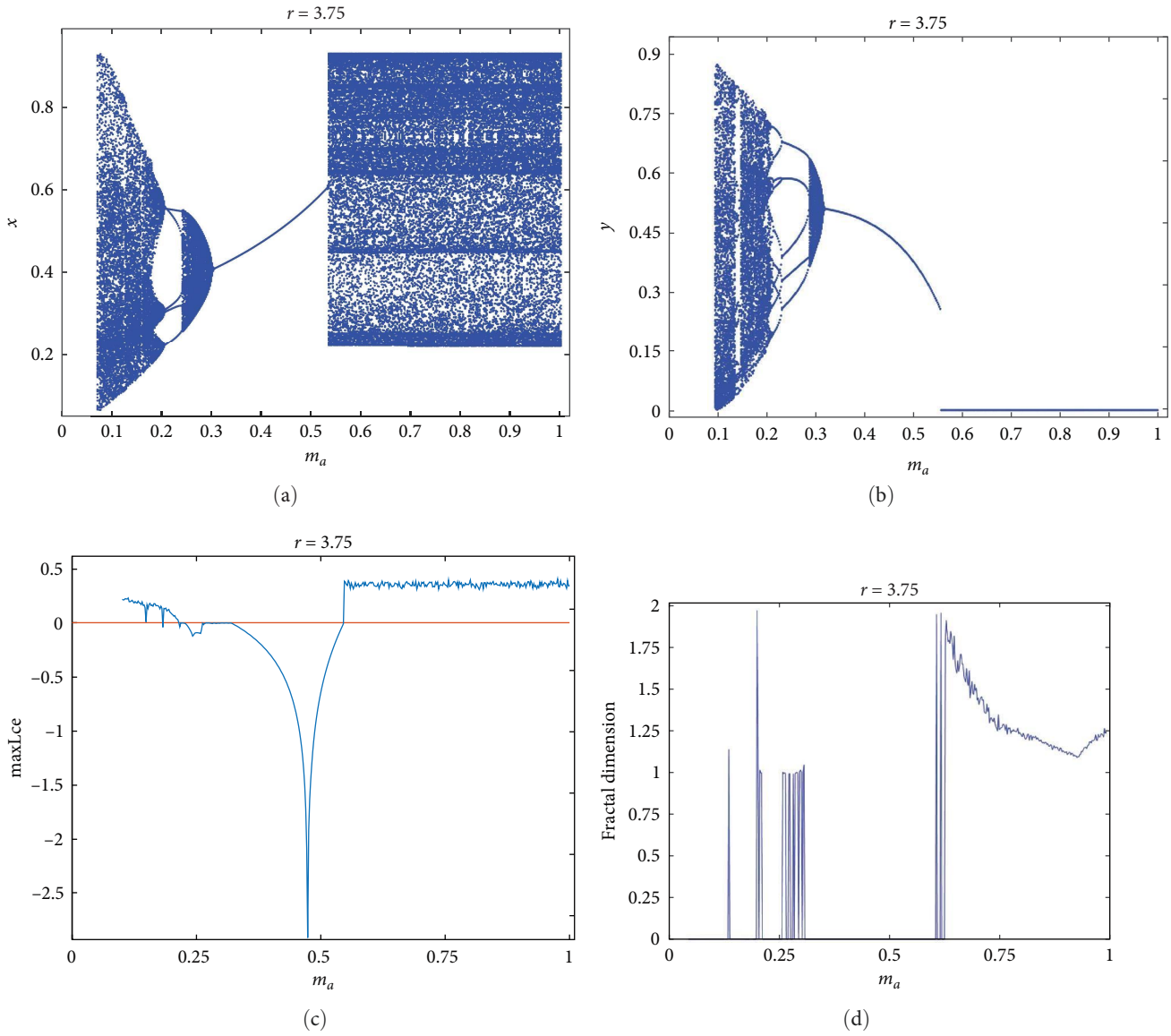

FIGURE 4: Visualization of NS bifurcation, MLEs, and FDs of species for changing parameter m_a for $r = 3.75$.

$0.23611 \pm 0.971726i$, and

$$\frac{d|\lambda_{ai}(m_a)|}{dm_a}\Big|_{m_a=m_{aNS}} = -2.52083 \neq 0,$$
$$-\left(tr\left(J_{\widetilde{M}_4}\right)\right)\Big|_{m_a=m_{aNS}} \neq 0 \Rightarrow = -0.472222 \neq 0, 1. \quad (31)$$

The Taylor coefficients are given by $\widehat{h}_{20} = -1.97917 - 0.483878i$, $\widehat{h}_{11} = 2.34375 - 4.79039i$, $\widehat{h}_{02} = 6.66667 + 5.478999i$, $\widehat{h}_{21} = 0$ and $s_2(m_{aNS}) = -39.0015$. The N–S bifurcation is supercritical as a result, which confirms Theorem 2.

The estimated and displayed maximum Lyapunov exponent for Figures 4(a) and 4(b) is shown in Figure 4(c). The chaotic zone has stable fixed points or stable periodic windows as a result of certain Lyapunov exponents being positive and some being negative, as shown in Figure 4(c). The diagrams, as shown in Figures 4(a) and 4(b), show that the fixed point $\tilde{\zeta}_2$ of the system (6) is unstable up to a scale factor of $m_a = 0.318182$ but becomes stable as the scale factor increases. The phase portraits associated with Figures 4(a) and 4(b) for various values of m_a are arranged in Figure 3, making it easy to see how a smooth invariant circle separates from the stable fixed point.

For scenario (iii), the bifurcation diagrams of system (6) in the $(\beta_a - x)$ and $(\beta_a - y)$ planes are shown in Figures 7(a) and 7(b) and corresponding MLEs and FDs are shown in Figures 7(c) and 7(d). Figure 8(a) shows the codimension-2 bifurcation diagrams in (β_a, m_a, x) space. The plot of the maximal Lyapunov exponents for two control parameters is shown in Figure 8(b) through a 2D projection onto the (β_a, m_a) plane.

5. Chaos Control

The state feedback method, pole placement methodology, OGY technique, and hybrid control approach are the most frequently used chaos control techniques for discrete-time

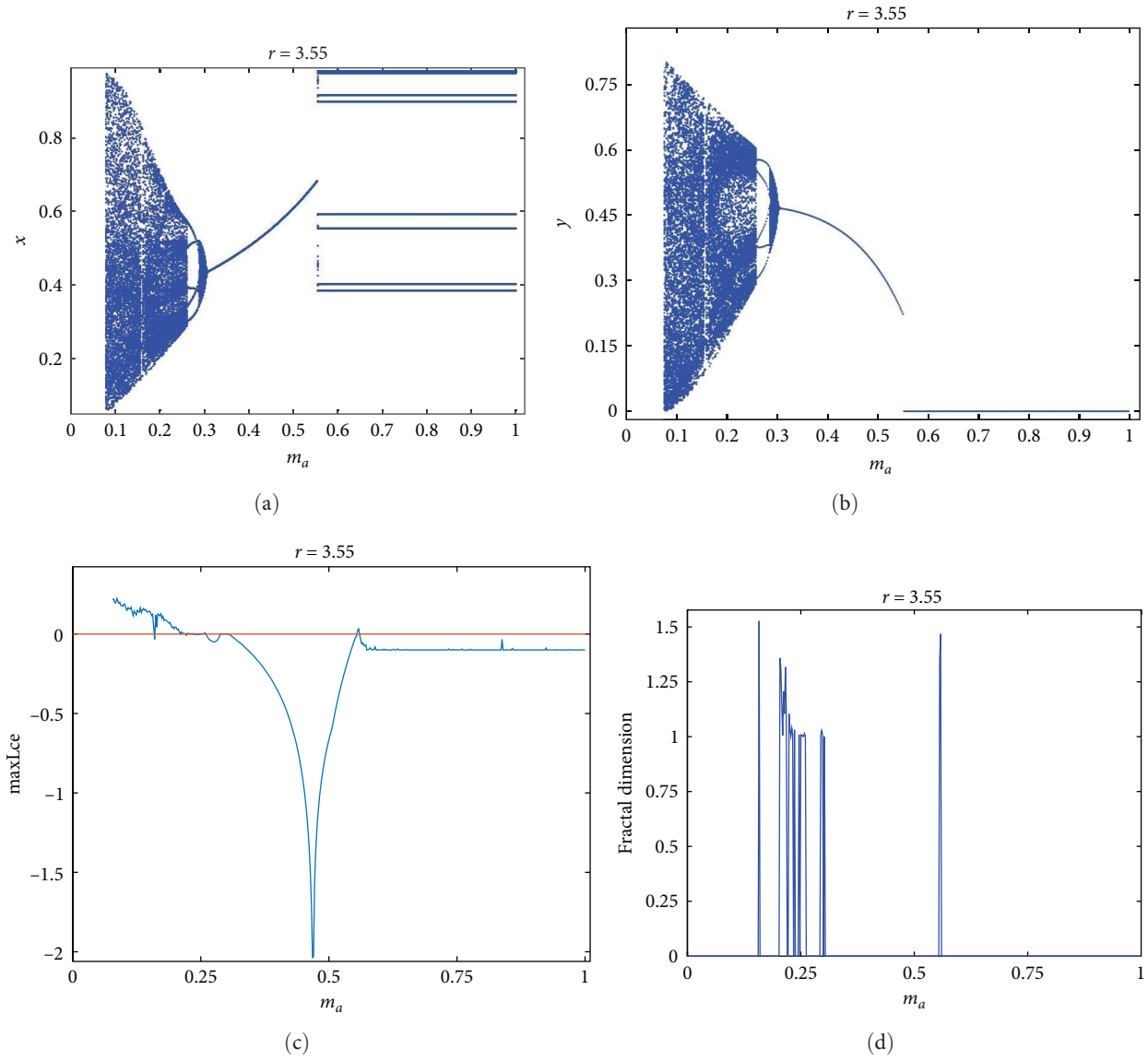

FIGURE 5: Visualization of NS bifurcation, MLEs, and FDs of species for changing parameter m_a for $r = 3.55$.

models. The chaos generated by N–S bifurcation, we apply the state feedback approach to control the chaos [43, 44] to the system (6) and using m_a as a control parameter. We write system (6) as follows:

$$x_{n+1} = rx_n(1 - x_n) - \alpha_a(1 - m_a)x_n y_n = f(x_n, y_n, m_a),$$
$$y_{n+1} = \beta_a(1 - m_a)x_n y_n - \delta_a y_n = g(x_n, y_n, m_a). \tag{32}$$

Then, the controlled form of system (32) can be written as follows:

$$x_{n+1} = rx_n(1 - x_n) - \alpha_a(1 - m_a)x_n y_n + \Lambda_n,$$
$$y_{n+1} = \beta_a(1 - m_a)x_n y_n - \delta_a y_n, \tag{33}$$

where the control force $\Lambda_n : = -k_1(x_n - x^*) - k_2(y_n - y^*)$ is specified as the feedback gains k_1 and k_2 and (x^*, y^*) is the interior fixed point for the system (6). The feedback gains k_1 and k_2 are critical in stabilizing and modifying the behavior of discrete dynamical systems under chaos control (see [44]). The goal of chaos control is to use control techniques to steer a chaotic system toward a desirable state or trajectory. The feedback gains k_1 and k_2 might be compared to regulatory mechanisms that restore the system to a stable state while making sure that critical processes stay within reasonable bounds. Similar to how biological systems are resilient to outside threats, k_1 and k_2 in chaos control can be seen as elements that contribute to the system's capacity to withstand disruptions and return to a desired state.

The following equation gives the Jacobian matrix W_c of the controlled system as follows:

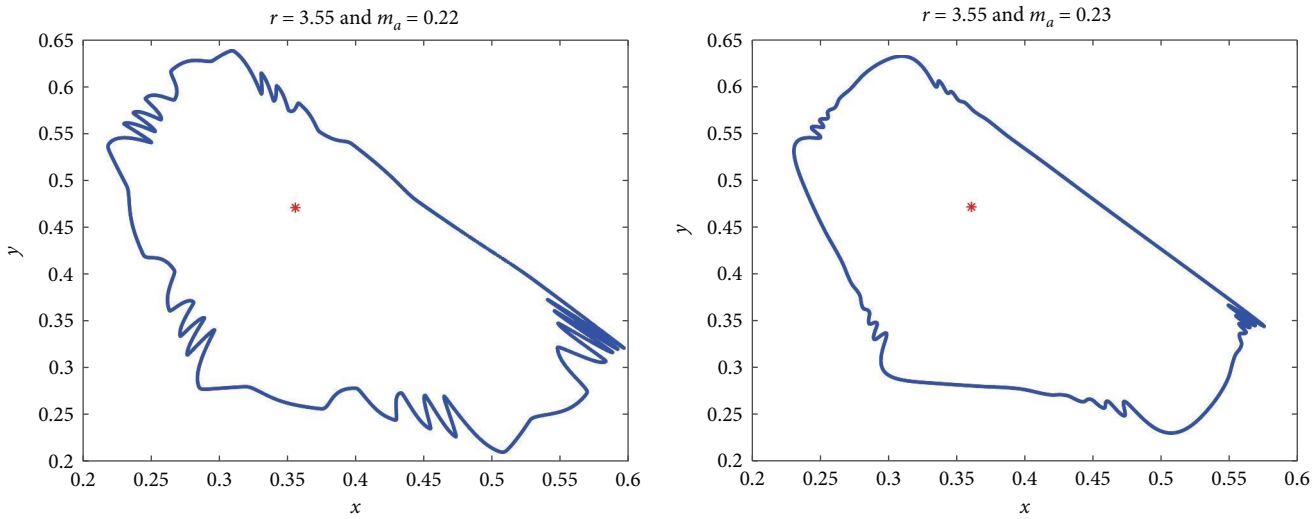

FIGURE 6: The phase diagram for altering the input of m_a. Red point inside the closed curve indicates system's fixed point.

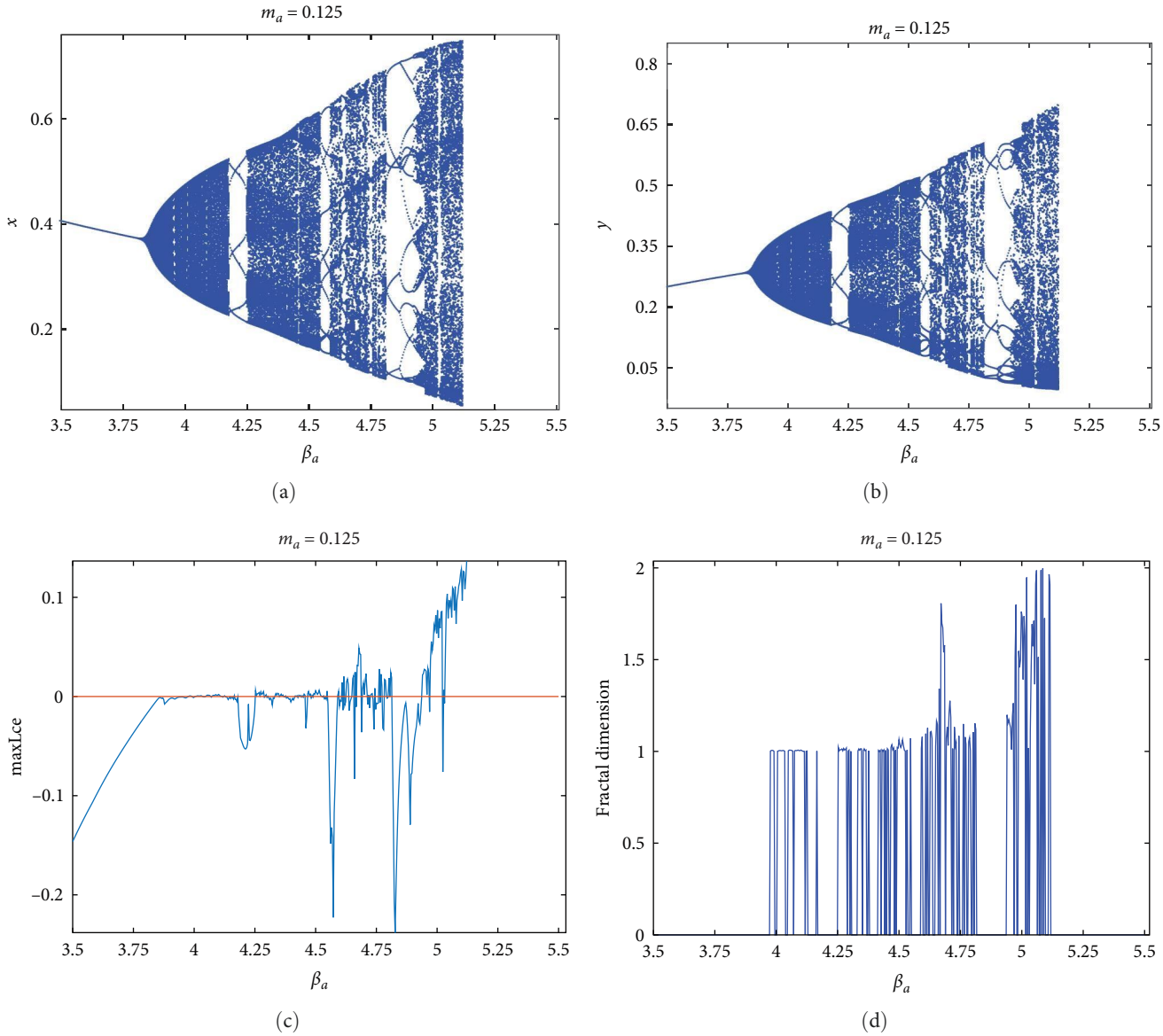

FIGURE 7: Visualization of NS bifurcation, MLEs, and FDs of species for changing parameter β_a.

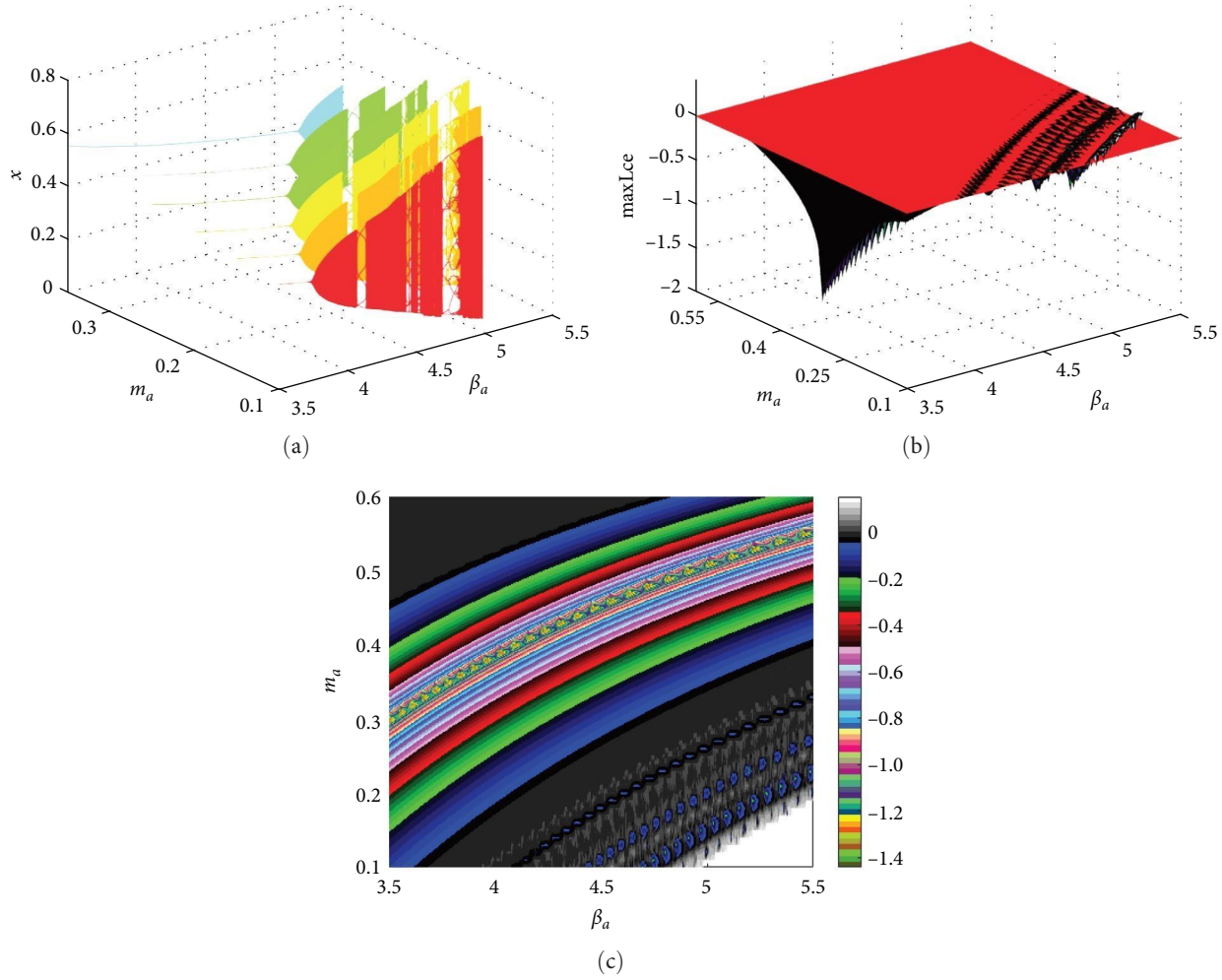

FIGURE 8: (a) Bifurcation diagram (3D) in (β_a, m_a, x) space. (b) 2D projection of 3D MLP. (c) Maximum Lyapunov exponents projected in two dimensions onto the (β_a, m_a) plane.

$$W_c(x^*, y^*) = \begin{pmatrix} \widetilde{w_{11}} - k_1 & \widetilde{w_{12}} - k_2 \\ \widetilde{w_{21}} & \widetilde{w_{22}} \end{pmatrix}, \tag{34}$$

where the values of $\tilde{w_{ij}}$, $i.j = 1, 2$ from (7) are determined at (x^*, y^*). The defining equation of (34) is shown as follows:

$$\lambda_a^2 - \widehat{p_{cc}}\lambda_a + \widehat{q_{cc}} = 0, \tag{35}$$

where $\widehat{p_{cc}} = (\tilde{w_{11}} + \tilde{w_{22}}) - k_1$ and $\widehat{q_{cc}} = (\tilde{w_{11}} - k_1)\tilde{w_{22}} - (\tilde{w_{12}} - k_2)\tilde{w_{21}}$. Let λ_{a1} and λ_{a2} represent the answers to (35).

Then,

$$\lambda_{a1} + \lambda_{a2} = \widehat{p_{cc}}, \tag{36}$$

and

$$\lambda_{a1}\lambda_{a2} = \widehat{q_{cc}}. \tag{37}$$

The marginal stability lines are obtained by solving the equations $\lambda_{a1} = \pm 1$ and $\lambda_{a1}\lambda_{a2} = 1$. These facts support the statement that $|\lambda_{a1}\lambda_{a2}| < 1$. Using (37) and assuming that $\lambda_{a1}\lambda_{a2} = 1$, we get as follows:

$$L_1 : \widetilde{w_{22}}k_1 - \widetilde{w_{21}}k_2 = \widetilde{w_{11}}\widetilde{w_{22}} - \widetilde{w_{12}}\widetilde{w_{21}} - 1. \tag{38}$$

Considering that $\lambda_{a1} = 1$, we obtain from (36) and (37) as follows:

$$L_2 : (1 - \widetilde{w_{22}})k_1 + \widetilde{w_{21}}k_2 = \widetilde{w_{11}} + \widetilde{w_{22}} - \widetilde{w_{11}}\widetilde{w_{22}} - 1 + \widetilde{w_{12}}\widetilde{w_{21}}. \tag{39}$$

Afterward, for $\lambda_{a1} = -1$, Equations (36) and (37) produce:

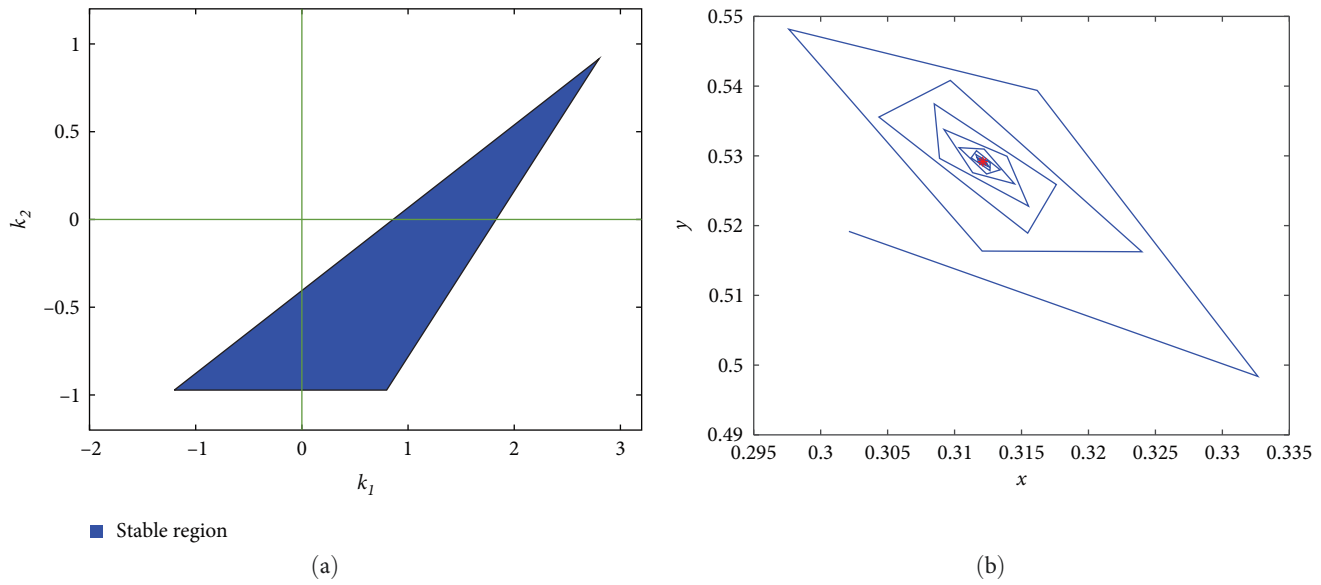

(a) (b)

FIGURE 9: Chaos regulation in system. (a) The stability zone in the (k_1, k_2) plane. (b) The regulated phase diagram.

$$L_3 : (1 + \widetilde{w_{22}})k_1 - \widetilde{w_{21}}k_2 = \widetilde{w_{11}} + \widetilde{w_{22}} + \widetilde{w_{11}}\widetilde{w_{22}} + 1 - \widetilde{w_{12}}\widetilde{w_{21}}. \tag{40}$$

As a result, the (k_1, k_2) plane's triangular region bounded by lines L_1, L_2, and L_3 (see Figure 9(a)) retains eigenvalues that fulfill $|\lambda_{a1}\lambda_{a2}| < 1$.

Let (x_0, y_0) be $(0.407407, 0.512169)$ and set other parameters as $\alpha_a = 3.5, \beta_a = 4.5, \delta_a = 0.25, r = 3.85$. From the stable region (triangular area) in (k_1, k_2) plane, as shown in Figure 9(a), we select the feedback gains as $k_1 = 1.0$ and $k_2 = -0.05$. It is then statistically shown that the chaotic trajectory is stabilized at the fixed point $(0.407407, 0.512169)$, as shown in Figure 9(b).

6. Conclusions

We examine the dynamics of a discrete predator–prey system utilizing a Holling type I functional response and a prey refuge. We determine the existence conditions and directions of the PD and N–S bifurcations near the interior fixed point of system (6) using the center manifold theory when the bifurcation parameter rises over a predetermined threshold. Notably, our results show that the model exhibits chaotic behavior and that the system becomes unstable when the parameter β_a increases, leading to a transition from a stable state to chaotic behavior. Also, the system becomes unstable when the parameter m_a increases. These demonstrate that the predator either falls extinct or reaches a stable fixed point when the dynamics of the prey are chaotic. Numerical estimates of the maximal Lyapunov exponents and the FD provide more evidence for the system's instability. Additionally, by varying the two control parameters, the system (6) displays extremely complex nonlinear dynamical behaviors and the chaotic phenomenon may be directly observed in the two-dimensional parameter spaces. Finally, the chaotic trajectory of the system has been controlled using the feedback control strategy. Despite this, resolving the system's numerous parameter, bifurcations remain a challenging task. More research on this topic should lead to more analytical conclusions, as we forecast.

Data Availability

There are no related data for this manuscript.

Conflicts of Interest

The authors declare that they have no conflicts of interest.

Authors' Contributions

The main findings were verified by all authors, who also gave their unanimous approval to the final manuscript.

References

[1] A. J. Lotka, "Elements of physical biology," *Nature*, vol. 116, Article ID 461, 1925.

[2] V. Volterra, "Variazioni e fluttuazionidelnumero di indivui in species animaliconviventi," *Memoria della Reale Accademia Nazionale dei Lincei*, vol. 2, pp. 31–313, 1926.

[3] J. F. G. Aguilar, "Behavior characteristics of a cap-resistor, memcapacitor, and a memristor from the response obtained of RC and RL electrical circuits described by fractional differential equations," *Turkish Journal of Electrical Engineering and Computer Sciences*, vol. 24, no. 3, pp. 1421–1433.

[4] A. Atangana and B. S. Talkahtani, "Extension of the resistance inductance capacitance electrical circuit to fractional

derivative without singular kernel," *Advances in Mechanical Engineering*, vol. 7, no. 6, pp. 1–6.

[5] J. F. Gómez-Aguilar, J. J. Rosales-García, J. J. Bernal-Alvarado, T. Córdova-Fraga, and R. GuzmánCabrera, "Fractional mechanical oscillators," *Revista Mexicana de Física*, vol. 58, no. 4, pp. 348–352, 2012.

[6] S. M. Salman, A. M. Yousef, and A. A. Elsadany, "Stability, bifurcation analysis and chaos control of a discrete predator-prey system with square root functional response," *Chaos, Solitons & Fractals*, vol. 93, pp. 20–31, 2016.

[7] A. Suryanto, I. Darti, H. S. Panigoro, and A. Kilicman, "A fractional-order predator–prey model with ratio-dependent functional response and linear harvesting," *Mathematics*, vol. 7, no. 11, Article ID 1100, 2019.

[8] R. Arditi and L. R. Ginzburg, "Coupling in predator-prey dynamics: ratio-dependence," *Journal of Theoretical Biology*, vol. 139, no. 3, pp. 311–326, 1989.

[9] C. Cosner, D. L. DeAngelis, J. S. Ault, and D. B. Olson, "Effects of spatial grouping on the functional response of predators," *Theoretical Population Biology*, vol. 56, no. 1, pp. 65–75, 1999.

[10] M. Danca, S. Codreanu, and B. Bakó, "Detailed analysis of a nonlinear prey-predator model," *Journal of Biological Physics*, vol. 23, no. 1, pp. 11–20, 1997.

[11] M. Fan and Y. Kuang, "Dynamics of a nonautonomous predator–prey system with the Beddington–DeAngelis functional response," *Journal of Mathematical Analysis and Applications*, vol. 295, no. 1, pp. 15–39, 2004.

[12] B. Liu, Y. Zhang, and L. Chen, "Dynamic complexities in a lotka–volterra predator–prey model concerning impulsive control strategy," *International Journal of Bifurcation and Chaos*, vol. 15, no. 2, pp. 517–531, 2005.

[13] D. Xiao and S. Ruan, "Global analysis in a predator-prey system with nonmonotonic functional response," *SIAM Journal on Applied Mathematics*, vol. 61, no. 4, pp. 1445–1472, 2001.

[14] W. Wang, Q.-X. Liu, and Z. Jin, "Spatiotemporal complexity of a ratio-dependent predator-prey system," *Physical Review E*, vol. 75, no. 5, Article ID 051913, 2007.

[15] H. N. Agiza, E. M. Elabbasy, H. El-Metwally, and A. A. Elsadany, "Chaotic dynamics of a discrete prey–predator model with Holling type II," *Nonlinear Analysis: Real World Applications*, vol. 10, no. 1, pp. 116–129, 2009.

[16] Q. Din, "Controlling chaos in a discrete-time prey-predator model with allee effects," *International Journal of Dynamics and Control*, vol. 6, no. 2, pp. 858–872, 2018.

[17] Q. Din, "Complexity and chaos control in a discrete-time prey-predator model," *Communications in Nonlinear Science and Numerical Simulation*, vol. 49, pp. 113–134, 2017.

[18] C. S. Holling, "The functional response of predators to prey density and its role in mimicry and population regulation," *Memoirs of the Entomological Society of Canada*, vol. 97, no. S45, pp. 5–60, 1965.

[19] K. Pusawidjayanti, Asmianto, and V. Kusumasari, "Dynamical analysis predator-prey population with holling type-II functional response," *Journal of Physics: Conference Series*, vol. 1872, no. 1, Article ID 012035, 2021.

[20] A. Q. Khan, "Neimark-Sacker bifurcation of a two-dimensional discrete-time predator-prey model," *SpringerPlus*, vol. 5, no. 1, Article ID 126, 2016.

[21] F. Kangalgil, "Neimark–Sacker bifurcation and stability analysis of a discrete-time prey–predator model with Allee effect in prey," *Advances in Difference Equations*, vol. 2019, no. 1, pp. 1–12, 2019.

[22] M. J. Uddin and C. N. Podder, "Fractional order prey–predator model incorporating immigration on prey: complexity analysis and its control," *International Journal of Biomathematics*, 2023.

[23] S. M. S. Rana, M. J. Uddin, P. K. Santra, and G. S. Mahapatra, "Chaotic dynamics and control of a discrete-time chen system," *Mathematical Problems in Engineering*, vol. 2023, Article ID 7795246, 20 pages, 2023.

[24] M. L. Rosenzweig and R. H. MacArthur, "Graphical representation and stability conditions of predator-prey interactions," *The American Naturalist*, vol. 97, no. 895, pp. 209–223, 1963.

[25] K. P. Hadeler and I. Gerstmann, "The discrete Rosenzweig model," *Mathematical Biosciences*, vol. 98, no. 1, pp. 49–72, 1990.

[26] X. Liu and D. Xiao, "Complex dynamic behaviors of a discrete-time predator–prey system," *Chaos, Solitons & Fractals*, vol. 32, no. 1, pp. 80–94, 2007.

[27] S. J. Maynard, *Models in Ecology*, Cambridge University Press, London, 1974.

[28] M. P. Hassel, *The Dynamics of Arthropod Predator-Prey Systems*, Princeton University Press, 1978.

[29] O. Anderson, "Optimal foraging by largemouth bass in structured environments," *Ecology*, vol. 65, no. 3, pp. 851–861, 1984.

[30] T. W. Anderson, "Predator responses, prey refuges, and density-dependent mortality of a marine fish," *Ecology*, vol. 82, no. 1, pp. 245–257, 2001.

[31] A. Sih, "Prey refuges and predator-prey stability," *Theoretical Population Biology*, vol. 31, no. 1, pp. 1–12, 1987.

[32] J. B. Collings, "Bifurcation and stability analysis of a temperature-dependent mite predator-prey interaction model incorporating a prey refuge," *Bulletin of Mathematical Biology*, vol. 57, no. 1, pp. 63–76, 1995.

[33] H. I. Freedman, *Deterministic Mathematical Models in Population Ecology*, Wiley, New York, 1980.

[34] E. González-Olivares and R. Ramos-Jiliberto, "Dynamic consequences of prey refuges in a simple model system: more prey, fewer predators and enhanced stability," *Ecological Modelling*, vol. 166, no. 1-2, pp. 135–146, 2003.

[35] M. E. Hochberg and R. D. Holt, "Refuge evolution and the population dynamics of coupled host? parasitoid associations," *Evolutionary Ecology*, vol. 9, no. 6, pp. 633–661, 1995.

[36] Y. Huang, F. Chen, and L. Zhong, "Stability analysis of a prey–predator model with holling type III response function incorporating a prey refuge," *Applied Mathematics and Computation*, vol. 182, no. 1, pp. 672–683, 2006.

[37] T. K. Kar, "Stability analysis of a prey–predator model incorporating a prey refuge," *Communications in Nonlinear Science and Numerical Simulation*, vol. 10, no. 6, pp. 681–691, 2005.

[38] V. Křivan, "Effects of optimal antipredator behavior of prey on predator–prey dynamics: the role of refuges," *Theoretical Population Biology*, vol. 53, no. 2, pp. 131–142, 1998.

[39] J. N. McNair, "The effects of refuges on predator-prey interactions: a reconsideration," *Theoretical Population Biology*, vol. 29, no. 1, pp. 38–63, 1986.

[40] S. Sarwardi, P. K. Mandal, and S. Ray, "Analysis of a competitive prey-predator system with a prey refuge." *Bio Systems*, vol. 110, no. 3, pp. 133–148, 2012.

[41] Y. A. Kuznetsov, *Elements of Applied Bifurcation Theory*, Springer, 1998.

[42] J. H. E. Cartwright, "Nonlinear stiffness, Lyapunov exponents, and attractor dimension," *Physics Letters A*, vol. 264, pp. 298–302, 1999.
[43] S. Elaydi, *An Introduction to Difference Equations*, Springer-Verlag, New York, 1996.
[44] S. Lynch, *Dynamical Systems with Applications Using Mathematica*, Springer, 2007.
[45] B. Ghosh, F. Grognard, and L. Mailleret, "Natural enemies deployment in patchy environments for augmentative biological control," *Applied Mathematics and Computation*, vol. 266, pp. 982–999, 2015.
[46] V. Seralan, R. Vadivel, D. Chalishajar, and N. Gunasekaran, "Dynamical complexities and chaos control in a ricker type predator-prey model with additive allee effect," *AIMS Mathematics*, vol. 8, no. 10, pp. 22896–22923, 2023.
[47] S. Vinoth, R. Vadivel, N.-T. Hu, C.-S. Chen, and N. Gunasekaran, "Bifurcation analysis in a harvested modified Leslie–Gower model incorporated with the fear factor and prey refuge," *Mathematics*, vol. 11, no. 14, Article ID 3118, 2023.
[48] S. Vinoth, R. Sivasamy, K. Sathiyanathan, B. Unyong, R. Vadivel, and N. Gunasekaran, "A novel discrete-time Leslie–Gower model with the impact of allee effect in predator population," *Complexity*, vol. 2022, Article ID 6931354, 21 pages, 2022.
[49] S. Vinoth, R. Sivasamy, K. Sathiyanathan et al., "The dynamics of a Leslie type predator–prey model with fear and allee effect," *Advances in Difference Equations*, vol. 2021, Article ID 338, 2021.
[50] G. P. Neverova, O. L. Zhdanova, B. Ghosh, and E. Y. Frisman, "Dynamics of a discrete-time stage-structured predator–prey system with Holling type II response function," *Nonlinear Dynamics*, vol. 98, no. 1, pp. 427–446, 2019.
[51] Rajni and B. Ghosh, "Multistability, chaos and mean population density in a discrete-time predator–prey system," *Chaos, Solitons & Fractals*, vol. 162, Article ID 112497, 2022.
[52] B. Ghosh, S. Sarda, and S. Sahu, "Torus doubling route to chaos and chaos eradication in delayed discrete-time predator–prey models," *Mathematical Methods in the Applied Sciences*, 2022.